






Evidence for Corotation Origin of Super-metal-rich Stars in LAMOST-Gaia: Multiple Ridges with a Similar Slope in the ϕ versus L_z Plane

Yuqin Chen^{1,2} , Gang Zhao^{1,2} , and Haopeng Zhang^{1,2} ¹ CAS Key Laboratory of Optical Astronomy, National Astronomical Observatories, Chinese Academy of Sciences, Beijing 100101, People's Republic of China; cyq@nao.cas.cn, gzhao@nao.cas.cn² School of Astronomy and Space Science, University of Chinese Academy of Sciences, Beijing 100049, People's Republic of China

Received 2022 July 10; revised 2022 August 2; accepted 2022 August 14; published 2022 August 29

Abstract

Super-metal-rich (SMR) stars in the solar neighborhood are thought to be born in the inner disk and come to their present location by radial migration, which is most intense at the corotation resonance (CR) of the Galactic bar. In this work, we show evidence for the CR origin of SMR stars in the Large Sky Area Multi-Object Fiber Spectroscopic Telescope and Gaia by detecting six ridges and undulations in the ϕ versus L_z space coded by median V_R , following a similar slope of $-8 \text{ km s}^{-1} \text{ kpc deg}^{-1}$. The slope is predicted by Monari et al.'s model for CR of a large and slow Galactic bar. For the first time, we show the variation in the angular momentum with azimuths from -10° to 20° for two outer and broad undulations with negative V_R around -18 km s^{-1} following this slope. The wave-like pattern with large amplitude outside CR and a wide peak of the second undulation indicate that minor merger of the Sagittarius dwarf galaxy with the disk might play a role besides the significant impact of the CR of the Galactic bar.

Unified Astronomy Thesaurus concepts: Galaxy disks (589); Galaxy evolution (594); Stellar kinematics (1608)

1. Introduction

With the release of the Gaia data, rich structures in the phase-space distribution have been revealed. For instance, multiple ridges displayed in the velocity space were found by Katz et al. (2019) and Ramos et al. (2018). Fragkoudi et al. (2019) also reported the ridge of the Hercules moving group, and many features, the so-called “horn” and “hat”, in the R versus V_ϕ coded by the mean V_R velocity. The origins of these rich structures is a debate topic with the Hercules moving group as a typical case. It has been suggested that the Hercules moving group, first reported in Dehnen (1999), was formed outside of the outer Lindblad resonance (OLR) based on a faster bar (Monari et al. 2016). However, Pérez-Villegas et al. (2017) favored for the scenario in which orbits trapped at the corotation resonance (CR) of a slow bar could produce the Hercules moving group in the local velocity space. Based on the Galactic model of Pérez-Villegas et al. (2017), Monari et al. (2019b) proposed that no fewer than six ridges in the local action space can be related to resonances of this slow bar, which induces a wave-like pattern with a wavenumber of $m = 6$ excitation. However, Friske & Schönrich (2019) explained the ridges in the average Galactocentric radial velocity as a function of the angular momentum and azimuth as a wavenumber $m = 4$ pattern caused by spiral arms.

Most of the observed structures in the phase-space distribution can be explained by different combinations of nonaxisymmetric perturbations, making their modeling degenerate (Hunt et al. 2019). Meanwhile, the relative contribution of the CR and OLR resonances (e.g., for the Hercules moving group) is different between the slow and fast rotation speed of the Galactic bar. The combination of different resonances due to various perturbations make it difficult to discover their origins.

Following the ridges as a function of the azimuth provides a promising way of disentangling the effect of different resonances. In this respect, Monari et al. (2019a) shows that the Hercules angular momentum changes significantly with the azimuth as expected for the CR resonance of a dynamically old large bar. They proposed that such a variation would not happen close to the OLR of a faster bar at least for 2 Gyr after its formation.

In this letter, we investigate the variation in the angular momentum (L_z) with the Galactic azimuth (ϕ) coded by V_R using super-metal-rich (SMR) stars in the Large Sky Area Multi-Object Fiber Spectroscopic Telescope (LAMOST)-Gaia survey as tracers. As SMR stars in the solar neighborhood are thought to originate from the inner disk (Chen et al. 2003; Kordopatis et al. 2015; Chen et al. 2019), features related to the CR resonance of the Galactic bar should be easily identified in this special population.

2. Data

SMR stars with $[\text{Fe}/\text{H}] > 0.2$ and spectral signal-to-noise ratios (S/N) larger than 10 are selected from LAMOST data release (DR) 7 (Zhao et al. 2006; Cui et al. 2012; Zhao et al. 2012; Deng et al. 2012; Liu et al. 2015), which provides the radial velocities and updated stellar parameters based on methods in Luo et al. (2015). Then we crossmatch this sample with Gaia early data release (EDR) 3 (Gaia Collaboration et al. 2021) to obtain proper motions and limit stars with errors in proper motions of less than 0.05 mas/yr and a renormalized unit weight error of $\text{RUWE} < 1.44$ (Lindegren et al. 2018). Bayesian distances are from the StarHorse code (Anders et al. 2019) using Gaia EDR3 and stars with relative errors less than 10% are adopted. The radial velocities are based on the LAMOST survey, and stars with errors in the radial velocity larger than 10 km s^{-1} are excluded from the sample.

The Galactocentric positions, spatial velocities, and orbital parameters (apocentric/pericentric distances, R_{apo} and R_{per}) are



Original content from this work may be used under the terms of the [Creative Commons Attribution 4.0 licence](https://creativecommons.org/licenses/by/4.0/). Any further distribution of this work must maintain attribution to the author(s) and the title of the work, journal citation and DOI.

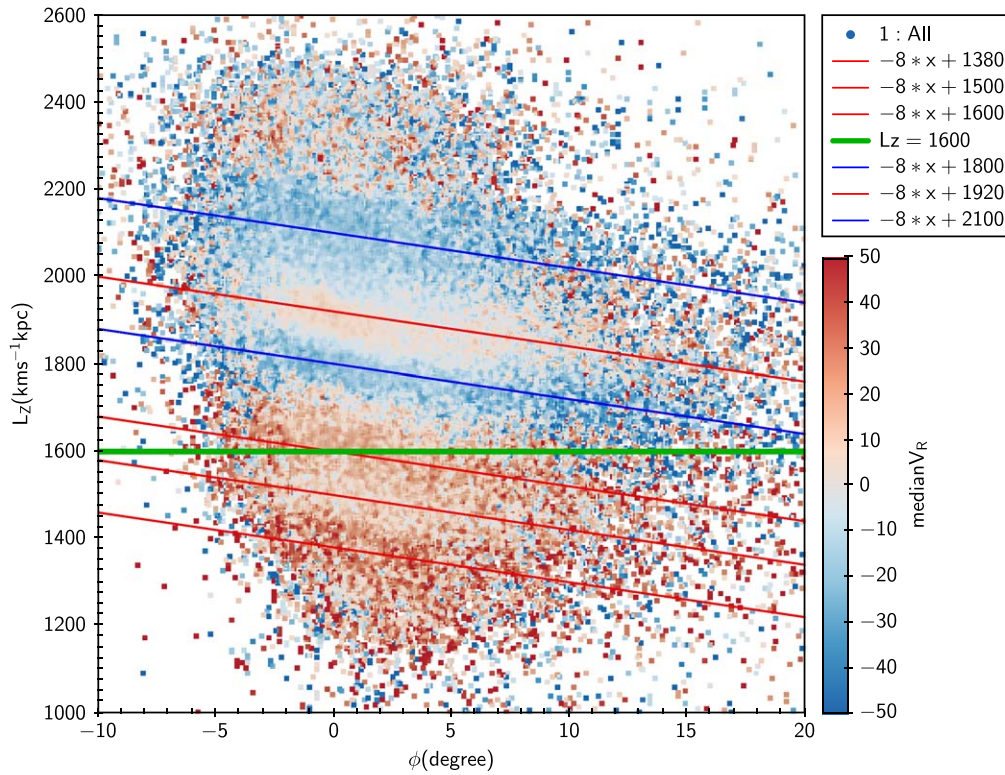


Figure 1. Median V_R in the ϕ vs. L_z space for SMR stars. The red lines for ridges (high V_R) and blue lines for undulations (low V_R) correspond to a slope of $-8 \text{ km s}^{-1} \text{ kpc deg}^{-1}$ (expected for CR), while the green line corresponds to $0 \text{ km s}^{-1} \text{ kpc deg}^{-1}$ (expected for OLR). Note that the red line of $L_z = -8\phi + 1600 \text{ km s}^{-1} \text{ kpc}$ corresponds to the location of the Hercules moving group as previously reported by Monari et al. (2019a).

calculated based on the publicly available code Galpot with the default potential (MilkyWayPotential) provided by McMillan (2017). Note that L_z are calculated with the definition of Equation (3.72) as presented in Binney & Tremaine (2008), while Monari et al. (2019a) adopted an approximate value of RV_ϕ . We use the cylindrical coordinate (V_R, V_ϕ, V_z) with the Sun’s distance from the Galactic center $R = 8.21 \text{ kpc}$, the solar peculiar velocity of $(U_\odot, V_\odot, W_\odot) = (11.1, 12.24, 7.25) \text{ km s}^{-1}$ (Schönrich et al. 2010) and the circular speed of $V_c = 233.1 \text{ km s}^{-1}$ (McMillan 2011). The sample has 214,199 stars with velocities between -300 km s^{-1} and $+300 \text{ km s}^{-1}$ and velocity dispersions of $(36.1, 23.1, 17.3) \text{ km s}^{-1}$ in (V_R, V_ϕ, V_z) . Their Galactic locations are $7 < R < 10 \text{ kpc}$ and $-0.5 < Z < 1.5 \text{ kpc}$ with peaks at $R = 8.5 \text{ kpc}$ and $|Z| \sim 0.25 \text{ kpc}$, respectively.

3. The ϕ versus L_z Plane

Figure 1 shows the ϕ versus L_z space coded by the median V_R for SMR stars. There are six ridges and undulations, generally following a similar slope of $-8 \text{ km s}^{-1} \text{ kpc deg}^{-1}$, which is predicted for stars with orbits trapped at CR in the Galactic model of Monari et al. (2019b). The red ridge with positive median V_R following the red line of $L_z = -8\phi + 1600 \text{ km s}^{-1} \text{ kpc}$ corresponds to the Hercules moving group in Monari et al. (2019a), and for comparison we plot the green line, which has a zero slope with $L_z = 1600 \text{ km s}^{-1} \text{ kpc}$ at $\phi = 0$, as expected for the OLR in the bar model. Note that the range of mean V_R in Monari et al. (2019a; their Figure 2) is of $\pm 20 \text{ km s}^{-1}$, while the coverage of $\pm 50 \text{ km s}^{-1}$ in median V_R is adopted in our Figure 1. The uncertainties of the median V_R for these features are of $0.5\text{--}1.0 \text{ km s}^{-1}$.

Except for the Hercules moving group, two ridges (with intercepts of 1380 and $1920 \text{ km s}^{-1} \text{ kpc}$) and three undulations (with intercepts of 1500 , 1800 , and $2100 \text{ km s}^{-1} \text{ kpc}$) are clearly shown. The similar slope in the L_z versus ϕ plane for the six ridges and undulations indicates that the bar’s resonance is not limited within the location of the Hercules moving group ($L_z = 1600 \text{ km s}^{-1} \text{ kpc}$) but has significant effect in the solar neighborhood ($L_z = 2100 \text{ km s}^{-1} \text{ kpc}$).

Meanwhile, positive median V_R values are found for the inner region of $L_z < 1700 \text{ km s}^{-1} \text{ kpc}$, above which median V_R values are negative except for a narrow ridge of $L_z = -8\phi + 1920 \text{ km s}^{-1} \text{ kpc}$ with median V_R of the order of 10 km s^{-1} . This transition may indicate that a minor merge event might start to take effect, which significantly increases the variation amplitude and makes the undulations wider. As the slope of $-8 \text{ km s}^{-1} \text{ kpc deg}^{-1}$ persists, we expect that the role of the CR is still significant in the outer region of $L_z > 1700 \text{ km s}^{-1} \text{ kpc}$ for SMR stars. Interestingly, Gaia Collaboration et al. (2022) found a somewhat similar velocity distribution with a lower velocity variation (see their Figure 16), but a change in the sign of the V_R velocity (as a function of the Galactocentric angle) at a radius of 10 kpc , in phase with the bar angle, is not seen in our SMR sample because only a small fraction of SMR stars in our sample could reach to 10 kpc .

Although the wave-like pattern between the ridges and undulations are found for both the inner and outer regions, but the amplitudes and the widths are different. The two blue undulations in the outer region have (negative) median V_R values of $\sim -18 \text{ km s}^{-1}$, while the two ridges in the inner disk have (positive) median V_R values around 21 km s^{-1} . The width of the outmost undulation at $L_z = 2100 \text{ km s}^{-1} \text{ kpc}$ is the

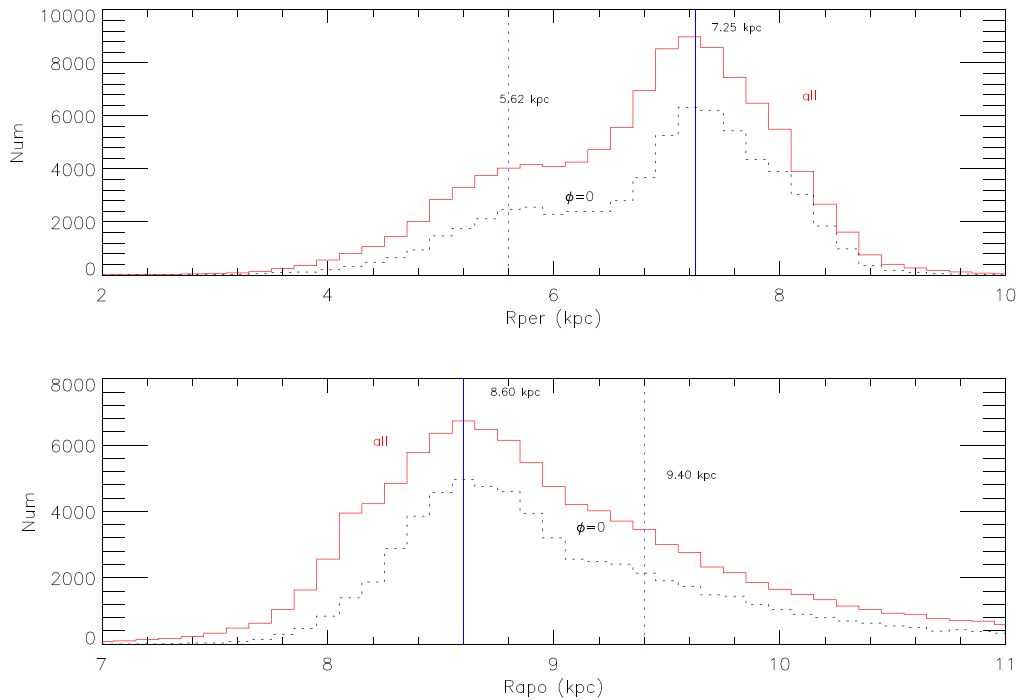


Figure 2. Distribution of pericenter and apocenter distances for all SMR stars (solid lines) and stars at the solar azimuth of $\phi \sim 0$ (dash lines). The blue lines are for the main (solid) and the second (dot) peaks in the distributions.

largest, spanning a range of 2.5 kpc from 7 to 9.5 kpc in terms of the guiding radius R_g , and the median V_R in the undulation is the most negative, which indicates that extra mechanisms, such as the minor merging of the Sgr dwarf galaxy, may have an important contribution to this undulation.

4. The Distributions of Pericenter and Apocenter Distances

In order to know how far these SMR stars can reach in the Galactic inner and outer disks, Figure 2 shows the distribution of pericenter and apocenter distances for all stars (red solid lines) and stars aligned with the Sun and the Galactic center (black dash lines). Then we fit the distributions with two Gaussian functions for stars at the solar azimuth ($\phi = 0$) and obtain two peaks for the pericenter and apocenter distances, respectively. The main peak of the pericenter distance is at 7.25 kpc, and there is a second peak at 5.62 kpc, while the histogram of the apocenter distance shows a main peak at 8.6 kpc and a second peak at 9.4 kpc. It is found that 79% SMR stars excuse within 4 kpc around the location of the Sun at 8.2 kpc. The second peak of the pericenter distance at 5.6 kpc is interesting because it is close to the CR position at 6 kpc in Pérez-Villegas et al. (2017) and very close to 5.5 kpc in Bovy et al. (2019) for a slow bar. There are 36% SMR stars with pericenter distances less than 6.5 kpc, and they are significantly affected by the CR of the Galactic bar. Finally, the apocenter distribution has a second peak at 9.4 kpc, which is within the the bar's OLR at about 10.5 kpc according to Pérez-Villegas et al. (2017).

5. Comparison with the Galactic Bar Model

Based on a realistic model for a slowly rotating large Galactic bar with a pattern speed of $\Omega_b = 39 \text{ km s}^{-1} \text{ kpc}^{-1}$, Monari et al. (2019b) showed no fewer than six ridges in the local action space that can be related to resonances with the bar.

It is interesting that SMR stars in the present sample do show six ridges and undulations in the L_z versus ϕ plane. For direct comparison, we adopt the Galactic coordinate frame for the stellar velocity (U, V, W) and show the $R-V$ diagram coded by the median $-U$ in Figure 3, which matches their Figure 6 quite well. Specifically, the ridge at L_z of 1380 corresponds to the CR (their green line) feature, and the undulation at $L_z = 2100 \text{ km s}^{-1} \text{ kpc}$ fits the OLR (their red line) feature. The two ridges (at 1600 and 1920 $\text{km s}^{-1} \text{ kpc}$) are associated with the 6:1 (pink) and 3:1 (purple) resonances, and one undulation at 1800 $\text{km s}^{-1} \text{ kpc}$ is related to the 4:1 (blue) resonance.

Note that the two ridges at $L_z = 1380 \text{ km s}^{-1} \text{ kpc}$ and $L_z = 1600 \text{ km s}^{-1} \text{ kpc}$ in the present work are the same as the strong positive V_R features near $L_z = 1400$ and $L_z = 1600$ observed in the solar neighborhood by Chiba & Schönrich (2021) based on Gaia DR2 as a result of the bar's resonance. They also suggested a slow bar with the current pattern speed of $\Omega_b = 35.5 \text{ km s}^{-1} \text{ kpc}^{-1}$ and placed the corotation radius at 6.6 kpc. Moreover, Chiba et al. (2021) introduced a decelerating bar model, which can reproduce with its corotation resonance the offset and strength of the Hercules stream in the local V_R versus V_ϕ plane and the double-peaked structure of the mean V_R in the $L_z-\phi$ plane due to the accumulation of orbits near the boundary of the resonance. Further work on the comparison of the model's result with observation is desire.

In summary, the multiple ridges and undulations found for SMR stars in Figure 1 can be explained by the bar resonances in the model of Monari et al. (2019b). Their similar slope indicates that these features (even in the OLR region) are affected by the CR of the slow and long bar. However, the strong V_R modulations from ridges to undulations and very wide range in the last undulation beyond the CR region suggest that minor merger may also play a role in the Galactic disk.

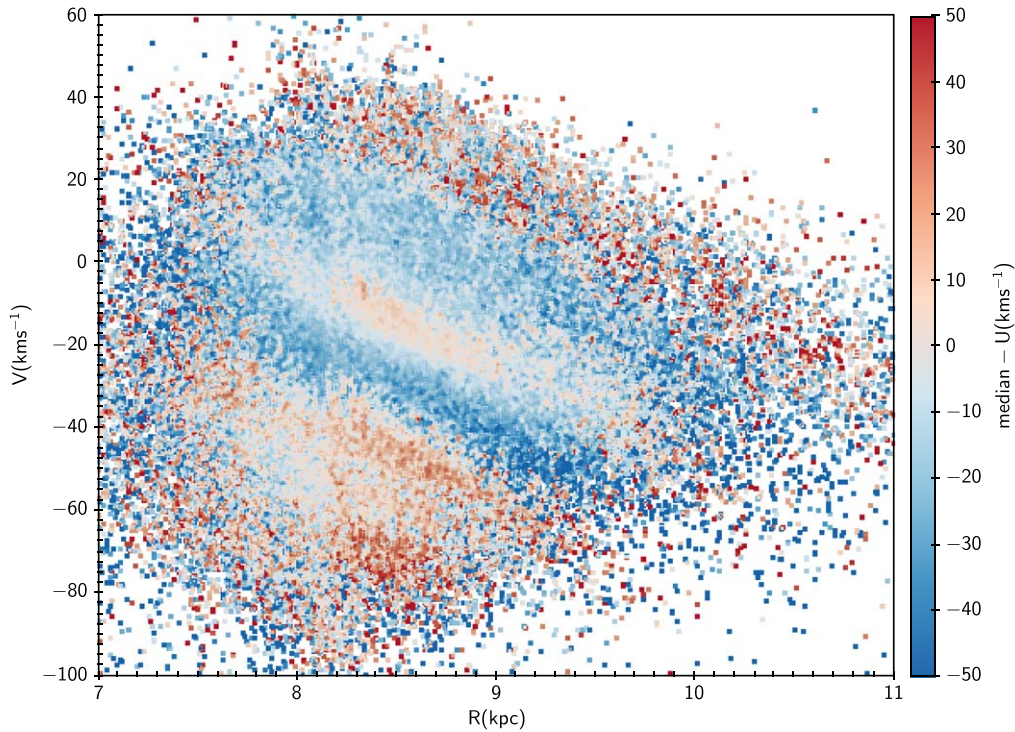


Figure 3. R vs. V coded by the median $-U$ for SMR stars. There is also a similar slope found for the six ridges and undulations.

Finally, we investigate chemical signatures of the six ridges and undulations based on abundances in Li et al. (2022), and there are 42,109 SMR stars with $[\text{Mg}/\text{Fe}]$ ratios available. There is no difference in $[\text{Mg}/\text{Fe}]$ among ridges and undulations. Both have a peak at $[\text{Mg}/\text{Fe}] \sim 0.05$ dex, typical for the old bar. Based on the LAMOST middle-resolution survey, Zhang et al. (2021) also suggested that SMR stars have slightly enhanced $[\text{Mg}/\text{Fe}] = 0.08$ dex. Note that stars from the Sgr dwarf galaxy itself usually have low $[\text{Mg}/\text{Fe}] \sim -0.05$ at $[\text{Fe}/\text{H}] \sim -0.4$, and there is no star with super-solar metallicity as shown in Figure 9 of Zhao & Chen (2021). Therefore, these SMR stars in the present work are not from the Sgr dwarf galaxy itself, but the minor merge event of the Sgr dwarf galaxy with the Galactic disk could induce strong modulations of V_R from ridges to undulations, and make the undulation at $L_z = 2100 \text{ km s}^{-1} \text{ kpc}$ become wider.



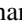
6. Conclusions

We have detected, for the first time, six ridges and undulations following a single slope in the ϕ versus L_z plane coded by the median V_R from a specific population of SMR stars based on LAMOST DR7 and Gaia EDR3. Specifically, the variation in the radial velocity with the angular momentum L_z and azimuth ϕ for the six ridges and undulations is seen with a similar slope of $-8 \text{ km s}^{-1} \text{ kpc deg}^{-1}$, which is predicted for stars with orbits trapped at the CR of a slow bar in the model of Monari et al. (2019b). The median V_R shifts from positive to negative values at $R_g \sim 7.4 \text{ kpc}$ (for $\phi = 0$, $L_z \sim 1700 \text{ km s}^{-1} \text{ kpc}$). This transition may indicate the role of minor merging starts to take effect together with the contribution from the CR of the bar. The most outer undulation around $R_g \sim 8.7 \text{ kpc}$ (for $\phi = 0$, $L_z \sim 2100 \text{ km s}^{-1} \text{ kpc}$) has a wide feature (three times larger than ridges), which is probably also related to the minor merge event of the Galactic disk with the Sgr dwarf galaxy, but this remains an open question for

further study in the future. Moreover, as the major merging event by the Gaia–Sausage–Enceladus galaxy bring its metal-rich component (Zhao & Chen 2021), and the accreted halo stars with special chemistry (Xing et al. 2019), into the solar neighborhood, it is interesting to probe how major merging events take effect on the existence of these ridges and undulations. Finally, many moving groups exist in the solar neighborhood (Zhao et al. 2009), and it is of high interest to probe if they may leave some imprints on the ϕ versus L_z plane coded by the median V_R as the Hercules moving group.

This study is supported by the National Natural Science Foundation of China under grant Nos. 11988101, 11890694, and National Key R&D Program of China under grant No. 2019YFA0405502. Guoshoujing Telescope (Large Sky Area Multi-Object Fiber Spectroscopic Telescope; LAMOST) is a National Major Scientific Project has been provided by the National Development and Reform Commission. LAMOST is operated and managed by the National Astronomical Observatories, Chinese Academy of Sciences. This work has made use of data from the European Space Agency (ESA) mission Gaia (<https://www.cosmos.esa.int/gaia>), processed by the Gaia Data Processing and Analysis Consortium (DPAC; <https://www.cosmos.esa.int/web/gaia/dpac/consortium>). Funding for the DPAC has been provided by national institutions, in particular the institutions participating in the Gaia Multilateral Agreement.

ORCID iDs

Yuqin Chen  <https://orcid.org/0000-0002-8442-901X>
 Gang Zhao  <https://orcid.org/0000-0002-8980-945X>
 Haopeng Zhang  <https://orcid.org/0000-0003-3265-9160>

References

- Anders, F., Khalatyan, A., Chiappini, C., et al. 2019, *A&A*, **628**, A94
- Binney, J., & Tremaine, S. 2008, *Galactic Dynamics: Second Edition* (Princeton, NJ: Princeton Univ. Press)
- Bovy, J., Leung, H. W., Hunt, J. A. S., et al. 2019, *MNRAS*, **490**, 4740
- Chen, Y. Q., Zhao, G., Nissen, P. E., Bai, G. S., & Qiu, H. M. 2003, *ApJ*, **591**, 925
- Chen, Y. Q., Zhao, G., Zhao, J. K., et al. 2019, *AJ*, **158**, 249
- Chiba, R., Friske, J. K. S., & Schönrich, R. 2021, *MNRAS*, **500**, 4710
- Chiba, R., & Schönrich, R. 2021, *MNRAS*, **505**, 2412
- Cui, X.-Q., Zhao, Y.-H., Chu, Y.-Q., et al. 2012, *RAA*, **12**, 1197
- Dehnen, W. 1999, *ApJ*, **524**, L35
- Deng, L.-C., Newberg, H. J., Liu, C., et al. 2012, *RAA*, **12**, 735
- Fragkoudi, F., Katz, D., Trick, W., et al. 2019, *MNRAS*, **488**, 3324
- Friske, J. K. S., & Schönrich, R. 2019, *MNRAS*, **490**, 5414
- Gaia Collaboration, Brown, A. G. A., Vallenari, A., et al. 2021, *A&A*, **649**, A1
- Gaia Collaboration, Drimmel, R., Romero-Gomez, M., et al. 2022, arXiv:2206.06207
- Hunt, J. A. S., Bub, M. W., Bovy, J., et al. 2019, *MNRAS*, **490**, 1026
- Katz, D., Sartoretti, P., Cropper, M., et al. 2019, *A&A*, **622**, A205
- Kordopatis, G., Wyse, R. F. G., Gilmore, G., et al. 2015, *A&A*, **582**, A122
- Li, Z., Zhao, G., Chen, Y., Liang, X., & Zhao, J. 2022, *MNRAS*, *Advance Access*
- Lindgren, L., Hernández, J., Bombrun, A., et al. 2018, *A&A*, **616**, A2
- Liu, X.-W., Zhao, G., & Hou, J.-L. 2015, *RAA*, **15**, 1089
- Luo, A. L., Zhao, Y.-H., Zhao, G., et al. 2015, *RAA*, **15**, 1095
- McMillan, P. J. 2011, *MNRAS*, **414**, 2446
- McMillan, P. J. 2017, *MNRAS*, **465**, 76
- Monari, G., Famaey, B., & Siebert, A. 2016, *MNRAS*, **457**, 2569
- Monari, G., Famaey, B., Siebert, A., et al. 2019a, *A&A*, **632**, A107
- Monari, G., Famaey, B., Siebert, A., Wegg, C., & Gerhard, O. 2019b, *A&A*, **626**, A41
- Pérez-Villegas, A., Portail, M., Wegg, C., & Gerhard, O. 2017, *ApJL*, **840**, L2
- Ramos, P., Antoja, T., & Figueras, F. 2018, *A&A*, **619**, A72
- Schönrich, R., Binney, J., & Dehnen, W. 2010, *MNRAS*, **403**, 1829
- Xing, Q.-F., Zhao, G., Aoki, W., et al. 2019, *NatAs*, **3**, 631
- Zhang, H.-P., Chen, Y.-Q., Zhao, G., et al. 2021, *RAA*, **21**, 153
- Zhao, G., & Chen, Y. 2021, *SCPMA*, **64**, 239562
- Zhao, G., Chen, Y.-Q., Shi, J.-R., et al. 2006, *ChJAA*, **6**, 265
- Zhao, G., Zhao, Y.-H., Chu, Y.-Q., Jing, Y.-P., & Deng, L.-C. 2012, *RAA*, **12**, 723
- Zhao, J., Zhao, G., & Chen, Y. 2009, *ApJL*, **692**, L113